Ecological Informatics 84 (2024) 102919

Contents lists available at ScienceDirect

Ecological Informatics

journal homepage: www.elsevier.com/locate/ecolinf

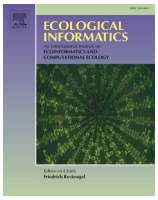

Study of underwater sound propagation and attenuation characteristics at the Yangjiang offshore wind farma

Xinze Huo, Peizhen Zhang *, Ziyi Feng

School of Electronics and Information Engineering, Guangdong Ocean University, Zhanjiang 524088, China

ARTICLE INFO

Keywords:
Offshore wind farm
Noise characteristics
Sound propagation
Sound attenuation

ABSTRACT

The rapid growth of offshore wind farms has become a global priority, with both new and total installed capacities increasing sharply. Consequently, underwater noise generated with these developments has garnered significant attention. This study investigated the signals produced by 5.5 MW wind turbines at the Yangjiang offshore wind farm, focusing on various distances and depths. Results showed that the primary energy of the underwater noise was concentrated below 1500 Hz. At the same distance, deeper waters had lower noise levels than shallower waters. The discrete spectrum near the wind farm has a dominant frequency of 44 Hz. The peak sound pressure levels reach 93.76 dB at a depth of 10 m and 81.55 dB at 20 m, measured 50 m from the turbine. Horizontally, the sound pressure level of the dominant frequency decreased consistently as the distance from the wind farm increased. The sound transmission loss within 1 km is less than 10 dB, reaching 16.39 dB at 4 km, with noise levels nearing ambient ocean noise. A segmented spectral wide-angle parabolic equation was used to simulate the spatial sound field of the underwater noise, considering seabed topography. The noise propagation and attenuation models were validated against the measured data. Understanding noise propagation and attenuation with distance is crucial for selecting suitable offshore wind farm locations. Mitigating the impact of elevated underwater noise on sound-dependent species is essential for their survival.

1. Introduction

A healthy marine environment is a critical aspect of conservation biology (Vegu and Stephen, 2024). As offshore wind farms enter the operational phase, the continuous generation of high-intensity broadband underwater noise has emerged as a significant source of concern for marine background noise (Rami et al., 2024). Currently, there is insufficient research on this emerging noise source, but it is clear that offshore wind farms inevitably affects the ecological conditions of surrounding marine areas. Therefore, in-depth studies on underwater noise during the operational phases of these wind farms are crucial.

The noise generated during the operational phase significantly impacts the underwater acoustic environment, persisting throughout the decade-long operational lifespan of wind farms (Su, 2023). This noise can propagate over several kilometers (Wahlberg and Westerberg, 2005), with its intensity increasing alongside higher wind speeds and larger turbine sizes (Andrea et al., 2021; Madsen et al., 2006). Yoon et al. (2023) revealed that underwater noise during the operational phase of wind turbines is significantly influenced by wind speed, rotor speed, and tower vibrations. Tougaard et al. (2020) developed a linear model to assess the relationship between the total sound pressure level (SPL) of turbine noise, distance, wind speed, and turbine size. Marmo et al. (2013) developed a noise effect model to identify the relative differences in underwater noise produced by different types of foundation piles. Reinhall and Dahl (2011) used the finite-element method (FEM) to simulate the sound propagation process and acoustic field distribution around foundation piles. Additionally, Bartłomiej et al. (2024) evaluated the effectiveness of three commonly used models ISO 9613-2, CNOSSOS-EU, and Nord2000, in predicting the low-frequency noise generated by wind farms in further studies on wind farm noise propagation models. Boško et al. (2023) examined the cumulative noise effects of multiple adjacent wind farms and proposed a noise propagation model to assess their regional impacts. De Oliveira et al. (2023) studied the impact of onshore wind farm noise on amphibian diversity in Brazil's tropical forests during the dry season. These results indicated that wind farm noise did not significantly affect species richness or composition but emphasized the importance of identifying potential threats to mitigate global amphibian decline. Similarly, He et al. (2023) examined the

* Corresponding author.
E-mail address: zhangpz@gdou.edu.cn (P. Zhang).

https://doi.org/10.1016/j.ecoinf.2024.102919
Received 18 August 2024; Received in revised form 23 November 2024; Accepted 24 November 2024
Available online 26 November 2024

effects of wind farm noise and vibrations on aquatic organisms at different distances emphasizing the need to consider ecological impacts when designing and operating wind farms. Southall et al. (2023) provided a framework for assessing the relative risk of human activities on marine animals, focusing activities that generate sound. This framework can be used to evaluate the risks posed to various species by offshore wind farms.

Underwater sound propagation is affected by the physical properties of the medium, and dynamic sound speed profiles in marine environments add uncertainty to the prediction of propagation characteristics. To address these challenges, researchers have developed various modeling methods and techniques. Early studies on pile driving noise during wind farm construction, treated the seabed as a fluid medium (Lippert and Lippert, 2012; Reinhall and Dahl, 2011). However, this approach overlooked the role of soil. In actual pile-soil-water interactions, soil conditions significantly influence the noise produced during driving (Peng et al., 2023). The model did not accurately reflect the elastic properties of the soil or the propagation characteristics of shear waves, resulting in an inadequate description of the acoustic energy dissipation and propagation pathways. To enhance accuracy, classical theories of elastic wave propagation in Biot's porous media (such as soil and rock) have replaced fluid representation, shifting the focus to soil mechanics (Tsouvalas, 2020). Subsequently, the concept of an elastic seabed was introduced and combined with Scholte waves, significantly improving the model's precision (Fricke and Rolfes, 2015). However, when considering operational noise from wind farms, the study primarily focused on mechanical vibrations causing underwater noise due to tower vibrations. Thus, treating the seabed as an acoustic fluid is considered to be acceptable (Zhu et al., 2020).

Wang et al. (2022) conducted a simulation study on the propagation loss field for a vertical line-array sound source in shallow water using a normal-mode model. Their research validated errors in noise propagation models at different frequencies and highlighted the impact of noise frequency characteristics on noise propagation. Sun et al. (2022) investigated the frequency characteristics and attenuation properties of noise from wind turbine units at varying wind speeds through simulations and testing, providing valuable references for noise prediction and development and reduction strategies. He et al. (2024) proposed a novel model order reduction technique for efficient computation of underwater sound propagation models in longitudinally invariant environments. Sergeev (2024) studied normal-mode models propagating along coasts in wedge-shaped seas, exploring energy leakage after reaching critical depths and revealing sound field propagation characteristics under complex boundary conditions. On the other hand, Feng et al. (2024) proposed a stochastic model based on ray theory for rapid estimation of sound field characteristics in ocean environments. However, these methods still face trade-offs between computational speed and accuracy in practical applications. The parabolic eq. (PE) method has rapidly developed since its introduction to ocean acoustics, favored for its balance between computational speed and accuracy. Thus, it has become one of the most widely used models for simulating medium- and low-frequency underwater sounds (Buckingham, 1992; Etter, 2018; Jensen et al., 2011). Subsequently, Tu et al. (2023) discretized a wide-angle PE model using the Chebyshev pseudospectral method. This extension allows the spectral algorithm to be applied to multilayered media and laterally inhomogeneous waveguides.

Existing research on the operational phase noise from wind farms has primarily focused on noise quantification and characteristic analyses. While some preliminary studies have explored the propagation distance of operational noise, precise data at various depths and distances remain limited. This study examined the time-frequency characteristics of noise signals at various depths and distances during wind farm operations using actual underwater noise data. The characteristics of the underwater noise propagation from a wind farm were modeled using a segmented spectral wide-angle parabolic equation. This model describes the relationship between the noise attenuation and distance across different frequency bands. Formulas for noise attenuation based on distance, depth, wind speed, and other variables were provided for the wind farm underwater noise in the test area. These formulas were validated using the measured data.

2. Study area and experimental methods

The study area is situated in the waters south of Nanpeng Island, Dongping Town, Yangjiang City, Guangdong Province, China. The water depth ranged from 22 to 31 m, with the closest distance to the shore being approximately 19.5 km and the farthest being approximately 35 km. The average annual wind speed in the area is at least 5.5 m/s. The study area is includes 55 wind turbines, each with a capacity of 5.5 MW. The layout of the study area is shown in Fig. 1, the black frame indicates the study area, the black dots represent the deployment locations of the hydrophones, and the" +' symbols indicate the positions of the measured single-pile wind turbines.

In June 2022, an underwater noise data collection experiment was conducted at the Yangjiang Nanpeng Island Wind Farm. On the day of the experiment, sea conditions were overcast with a southeastern wind at Force 3 and moderate waves. A REASON TC4037 hydrophone was used for data acquisition, which has a sensitivity of approximately −192 dB, an instrument gain of 40 dB, and a sampling frequency of 100 kHz. The equipment was calibrated before the experiments. Upon reaching the designated area, the vessel's engine was turned off. The self-contained hydrophone was then deployed in the water for data collection. Two hydrophones were deployed at depths of 10 m and 20 m see Fig. 2. The test stations were located 50 km, 200 km, 500 km, 1 km, 4 km, and 8 km away from the wind turbine foundation.

According to the Acoustic Underwater Noise Testing Standard 5.4 specified in GBT 5262–2009 (General Administration of Quality Supervision, 2009), the data recording duration can be determined based on actual requirements, but generally should not be less than 2 min. In the experiment, the measurement duration at each station was approximately 20 min. The specific deployment times and locations of the hydrophones are listed in Table 1.

3. Experimental results and discussion

The time-frequency characteristics of underwater signals across different frequency bands are described using a Short-Time Fourier Transform (STFT). This involved analyzing the spectral response of the noise data at various distances.

3.1. Time-frequency characteristics of underwater signals

Fig. 3 illustrates the time-frequency characteristics of the underwater environmental noise measured around the offshore wind farm. Fig. 3(a) corresponds to a depth of 10 m, while (b) correspond to depth of 20 m. The horizontal axis represents the data collection duration, while the vertical axis represents the frequency, and the brightness of the image reflects the sound pressure level. Time-frequency spectrograms show that high-brightness regions are concentrated in the 20–1500 Hz frequency range, exhibiting distinct sideband-like patterns. The brightness values vary based on the distance from the wind farm.

At the first station, 50 m from the wind farm, the sound pressure level within this frequency band was highest, with a peak sound pressure level of approximately 1050 Hz. As the testing location moved from station b to station c, the distance increased from 200 to 500 m. The sound pressure level decreased significantly, though the peak center frequency remained unchanged. At stations d, e, and f, ranging from 1 to 8 km, results showed significant wind turbine noise even 1 km from the wind farm. Broadband signals were still observable at 4 km from the wind farm, but at 8 km, noise levels matched the background noise of the marine environment. This phenomenon of significant attenuation with increasing distances was consistent across different depths. At a depth of

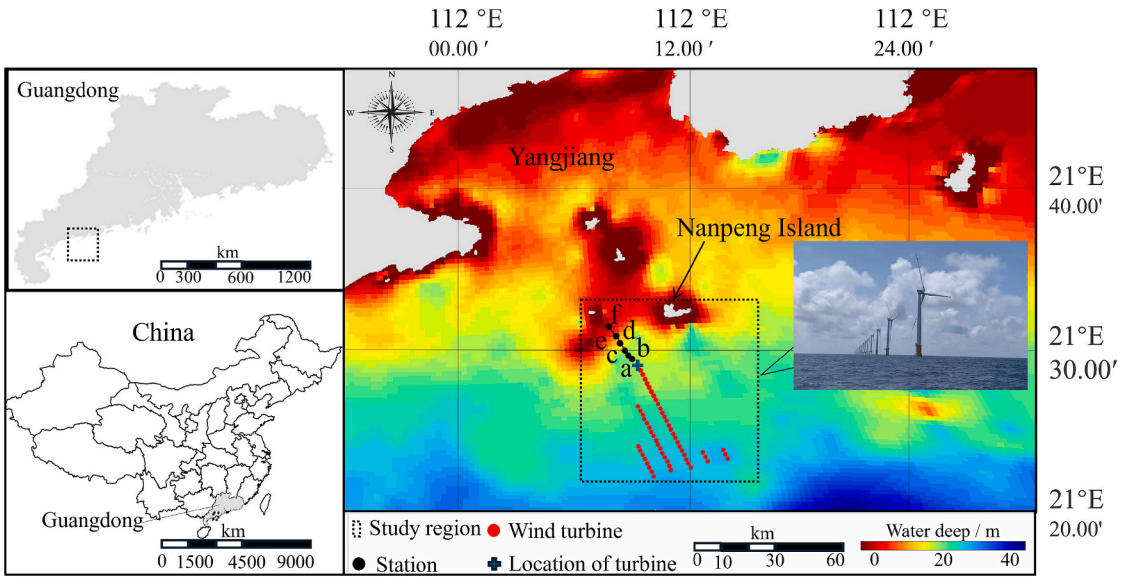

Fig. 1. Schematic of the study area (red area represents the wind farm; a, b, c, d, e, f denotes data collection locations). (For interpretation of the references to colour in this figure legend, the reader is referred to the web version of this article.)

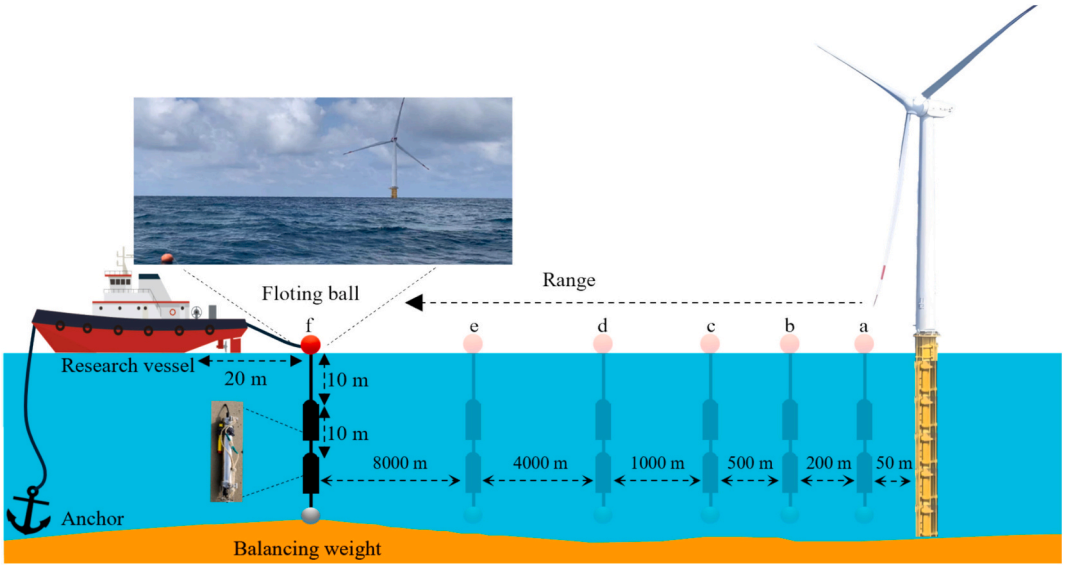

Fig. 2. The deployment of the hydrophone.

Table 1
Data collection records.

Date	Observation Station	Start Time	End Time	Station Latitude and Longitude
June 5, 2022	a(50 m)	14:10	14:30	21°29′42″N; 112°11′34″ E
	b(200 m)	15:02	15:23	21°30′15″N; 112°11′11″E
	c (500 m)	15:59	16:21	21°30′01″N; 112°11′18″E
	d(1 km)	15:02	15:23	21°31′10″N; 112°10′40″E
	e(4 km)	16:33	16:57	21°32′01″N; 112°09′44″E
	f(8 km)	17:08	17:37	21°33′24″N; 112°08′55″E

20 m, both the marine background noise and the wind farm signal noise were significantly lower than those at 10 m. This is because the wind-induced noise decreases with depth, especially when the wind speed exceeds the cut-in speed of 3 m/s, owing to significant vertical attenuation.

Similarly, throughout the underwater observation period, distinct discrete signals were evident when the frequency was below 500 Hz. These signals exhibited significant attenuation with increasing distance, consistent with the trend of the skirt-like spectrum as distance varied. Within a range of 4 km from the wind farm, the effects of the wind farm could still be detected, and discrete spectral components remained observable at the 4 km measurement station.

3.2. Frequency domain characteristics of underwater noise in offshore wind farms

The average power spectra of the time-domain signals were

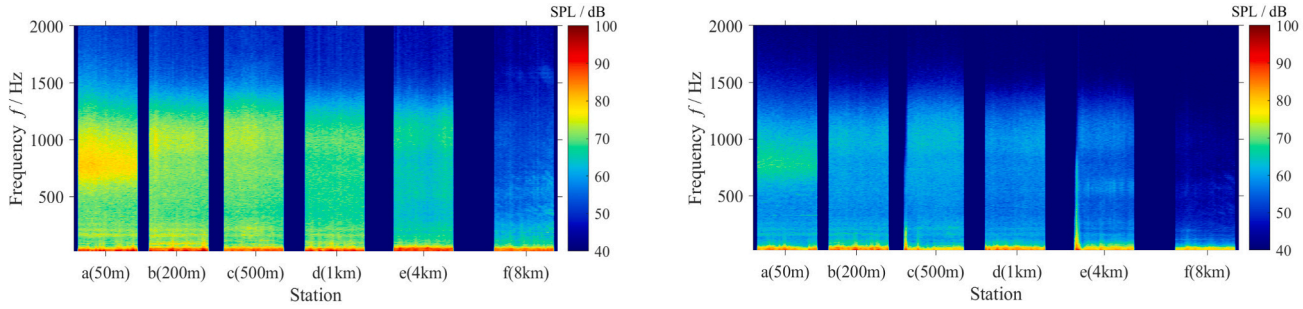

Fig. 3. Offshore wind farm noise time-frequency diagram: (a)10 m; (b)20 m.

calculated for six stations located at various depths. This demonstrates how the intensity of underwater environmental noise varies with frequency at the Yangjiang wind farm. In Fig. 4, the horizontal axis represents frequency, while the vertical axis represents noise sound pressure level. The sound pressure levels at 10 and 20 m depth decreased as the distance from the source increased. At a depth of 10 m, the dominant frequency at all six stations was 44 Hz. The peak sound pressure levels were 93.76, 91.78, 88.91, 87.02, 84.90, and 73.33 dB, respectively. At a depth of 20 m, the peak sound pressure levels were 81.55, 80.39, 76.20, 75.70, 72.40, and 60.43 dB, respectively. It is evident that the sound pressure level at a depth of 20 m is considerably lower than that at 10 m. This is primarily because the study area lies on the shallow continental shelf of the South China Sea, which has a typical negative-gradient sound speed structure (Wang et al., 2014). In this scenario, when sound rays reflected off the seabed, sound rays at large grazing angles, they often exceed the critical angle, leading to a significant increase in the seabed reflection loss. In shallow-water environments, variations in temperature with depth can lead to the formation of a thermocline. The thermocline can guide sound waves towards the surface or cause refraction, resulting in the "focusing" of noise near the sea surface, which increases the noise intensity (Liu et al., 2021). The primary frequencies of the signals were < 1500 Hz. The signal energy exhibited significant attenuation as the distance increased. Within a 4 km radius from the wind farm, the influence of the wind farm was detectable in the20–1500 Hz frequency bands. The overall sound pressure levels were noticeably higher than those of the ambient marine noise.

Fig. 3 and Fig. 4 indicate that the fundamental frequency of gear meshing in the wind turbine is 44 Hz, with discrete spectra exhibiting approximate harmonic relationships. The fundamental frequency of the generator's electromagnetic interactions is 103 Hz, higher than the gear meshing frequency. Additionally, mechanical noise can be amplified because of resonance effects within the wind turbine's internal structure. When the excitation frequency matches the harmonic frequency of the structural vibration, resonance occurs, leading to a significant increase in amplitude. Even very small excitation force amplitudes can amplify the structural response during resonance, resulting in high noise levels, consistent with the sideband-like spectral patterns observed in our measurements.

Based on the data presented in Fig. 4, the typical transmission a loss at various stations at different distances were analyzed. Relative to the reference sound energy at 50 m, the transmission loss for each station was calculated using the formula $TL = 10 \times \log10(E_1/E_2)$, where E_1 is the sound energy at 50 m, and E_2 is the sound energy at each of the six stations (a–f). This method allowed us to quantify the attenuation characteristics of the sound waves over different distances using the calculated results presented in Table 2.

Table 2
Transmission loss.

Depth (m)	Frequency (Hz)	Transmission loss (dB)					
		a(50 m)	b(200 m)	c(500 m)	d(1 km)	e(4 km)	f(8 km)
10	44	0	1.98	4.85	6.74	8.86	20.43
	88	0	0.85	3.37	7.22	10.24	19.36
	103	0	1.29	4.37	7.55	7.84	19.76
	176	0	1.35	6.73	9.68	14.81	24.34
	206	0	0.65	3.85	6.95	12.84	23.03
	1050	0	1.57	6.15	8.61	16.39	31.41
20	44	0	1.16	5.35	5.85	9.15	21.12
	88	0	2.15	4.41	8.56	10.50	20.15
	103	0	1.32	3.18	6.55	12.20	18.69
	176	0	2.76	6.90	9.21	7.33	25.81
	206	0	1.30	5.02	7.32	14.21	23.57
	1050	0	1.51	6.02	6.82	16.03	27.52

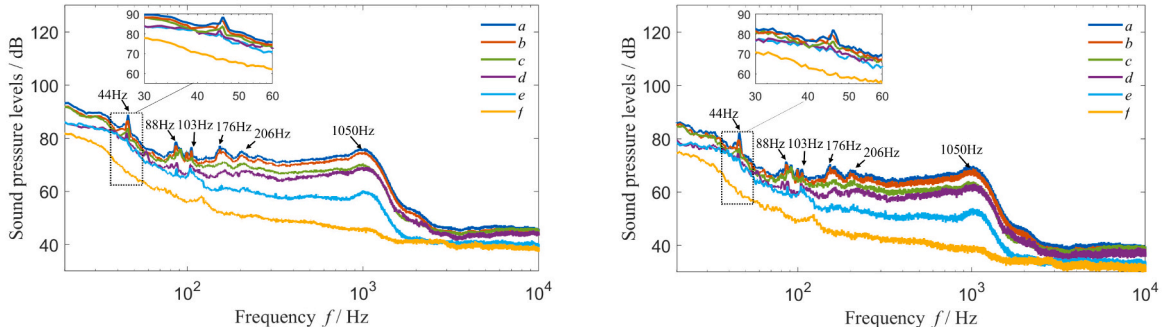

Fig. 4. Underwater noise frequency domain display in offshore wind farms: (a)10 m; (b)20 m.

In the preliminary data analysis, we found that the underwater sound intensity from the wind farm is primarily concentrated below 1500 Hz. The sound energy decreases as the water depth increases. This observation is consistent with the findings in the literature (Andersson, 2011; Betke et al., 2005; Lou and Ma, 2024; Qian et al., 2022; Wang et al., 2024). The sound pressure levels of wind farm noise attenuate significantly with distance. However, distinct discrete spectral lines are still observed within a 4-km range. To confirm that these signals originate from the wind farm's operation and to study how they vary with distance, we will use the Parabolic Eq. (PE) for comparison and analysis.

4. Sound propagation and attenuation characteristics

The parabolic equation model, based on asymptotic approximation, simplifies the Helmholtz equation into a parabolic equation and solves it using numerical methods. This model effectively addresses boundary issues in complex environments during far-field and large-angle propagation, offering high accuracy over long ranges and low computational costs (Gilbert and White, 1989). However, the solution of the parabolic equation is valid only within a range of angles close to the main propagation direction and neglects backward scattering. Nevertheless, this model demonstrated good accuracy in handling low-frequency wave propagation, making it highly suitable for simulating low-frequency noise propagation (Colas et al., 2023). This section introduces a solution to the parabolic equation using Chebyshev polynomials. To investigate the underwater propagation characteristics of wind turbine noise, we modeled the undulating seabed as a series of flat segments. Chebyshev spectral polynomials were then used to solve the PE for sound propagation across the seafloor. The introduction of mixed solution methods and adaptive spectral expansion techniques enhances the flexibility of the derivation process and improves the computational efficiency.

4.1. Spectral PE equation model

As shown in Fig. 5, a continuously undulating seabed was represented by a combination of multiple flat seabed segments. The underwater sound propagation medium is divided horizontally into l layers (h_1, h_2, …, $h\ell$, …, h_l). where h_{l-1} represents the seabed, denoted by H, and h_l represents the homogeneous acoustic half-space below the seabed, denoted by D.

For a horizontally stratified flat seabed, where $c\,(r, z)$, $\rho\,(r, z)$ and $\alpha\,(r, z)$ represent the sound speed, density, and attenuation coefficient of the medium, respectively, the underwater sound propagation medium is horizontally divided into layers. According to the split-step Padé wide-angle PE algorithm proposed by Collins (1993) and Collins (1994), the PE equation in cylindrical coordinates satisfies the following equation.

$$\frac{\partial^2 p}{\partial r^2}+\rho\frac{\partial}{\partial z}\left(\frac{1}{\rho}\frac{\partial p}{\partial z}\right)+k^2 p=0 \tag{1}$$

In Eq. (1) ρ, z, r represents the density, source depth, and propagation distance, respectively. The wavenumber k is given by $k = 2\pi(1 + i\,\eta\alpha)\,\omega/c$, where ω is the angular frequency, c is the sound speed, α is the attenuation coefficient, and $\eta = (40\pi\log_{10}^{e})^{-1}$. After factorization and considering only forward propagation, the split-step expansion yields the following form:

$$p(r+\Delta r, z)=exp(ik_0\Delta r)\prod_{j=1}^{n}\frac{1+a_j\chi}{1+b_j\chi}p(r,z) \tag{2}$$

In Eq. (2), $p\,(r, z)$ represents the sound pressure corresponding to distance and depth, n is the order of the Padé approximation, and a_j and b_j are the coefficients of the Padé approximation, with $\chi = k_0^2[\rho(\partial/\partial z)\,(1/\rho)\,(\partial/\partial z) + k^2 - k_0^2]$, $k_0 = 2\pi f/c$. The sea surface was set as a fully reflective boundary, and the uniform half-space D is treated as a perfectly matched layer. The spectral coefficients were obtained using Chebyshev polynomials as basic functions (Tu et al., 2022). According to the Chebyshev polynomial $u(t)$, which is a smooth function in the interval $t\in[-1,1]$, the approximate expansion is given as follows:

$$u(t)=\sum_{s=0}^{\infty}\widehat{u}_s T_s(t)\simeq\sum_{s=0}^{N}\widehat{u}T_s(t) \tag{3}$$

Eq. (3) $\{\hat{u}\}$ represents the spectral coefficients of $u(t)$, where N is the order of the spectral stage. As N increases, the error decreased exponentially. Based on the orthogonality of the Chebyshev polynomials, the spectral coefficients are expressed by Eq. (4).

$$\widehat{u}_s\simeq\frac{1}{d_s}\sum_{j=0}^{N}u(t_j)T_s(t_j)w_j,\ \ j=0,1,2,\ldots\ldots,N \tag{4}$$

The Gauss–Chebyshev–Lobatto quadrature was employed to improve the computational accuracy of Eq. (3), the Gauss-Chebyshev-Lobatto quadrature is employed. The Gaussian–Chebyshev–Lobatto nodes and weights are expressed as:

$$t_j=cos\left(\frac{j\pi}{N}\right),j=0,1,2,\ldots\ldots,N;w_j=\begin{cases}\dfrac{\pi}{2N},j=0,N,\\ \dfrac{\pi}{N},j\neq 0,N,\end{cases};\quad d_s$$

$$=\begin{cases}\pi,s=0,N,\\ \dfrac{\pi}{2},j\neq 0,N.\end{cases}$$

Function $u(t)$, based on the Chebyshev polynomials and their derivatives, yields the following relationship:

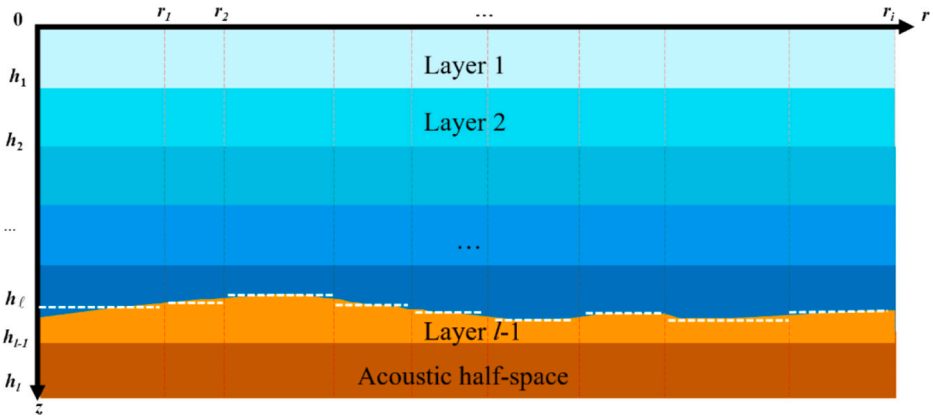

Fig. 5. Multi-layer media in undulating seabed.

$$u(t) = \sum_{s=0}^{\infty} \widehat{u}_s' T_s(t) = \left(\sum_{s=0}^{\infty} \widehat{u}_s T_s(t) \right)' = \sum_{s=0}^{\infty} \widehat{u}_s T_s'(t) \tag{5}$$

$$\widehat{u}_s' \simeq \frac{2}{c_s} \sum_{\substack{m=s+1, \\ m+s=odd}}^{N} m\widehat{u}_m,$$
$$\widehat{\mathrm{u}}' \simeq \mathrm{D}_N \widehat{\mathrm{u}} \tag{6}$$

Eq. (6) represents the matrix-vector form of the derivative relationship, where D_N is the $N+1$ order Legendre matrix, and $\hat{u}$ is the column vector composed of $\{\hat{u}_s\}_{s=0}^{N}$. The spectral coefficients of the product of the two functions have the following relationship:

$$\widehat{vu}_t \simeq \frac{1}{2} \sum_{m+n=s}^{N} \widehat{u}_m \widehat{v}_n + \frac{1}{2} \sum_{|m-n|=s}^{N} \widehat{u}_m \widehat{v}_n,$$
$$\widehat{\mathrm{vu}} \simeq \mathrm{C}_v \widehat{\mathrm{u}} \tag{7}$$

In Eq. (7), C_v is the coefficient matrix. When discretizing the wide-angle PE model using the Chebyshev spectral method, the solution domain $[z_1, z_2]$ is first scaled to $[t_1, t_2]$ before performing the spectral transformation, where $t = (2z)/(z_2 - z_1) - (z_2 + z_1) / (z_2 - z_1)$, $\mathrm{d}t/\mathrm{d}z = 2/(z_2 - z_1)$. The density ratio χ in Eq. (2) is discretized, resulting in the Chebyshev spectral space discrete form as follows:

$$\chi = k_0^{-2} \left[\frac{4}{\Delta z_i^2} p(t) \frac{\partial}{\partial t} \left(\frac{1}{p(t)} \frac{\partial}{\partial t} \right) + k^2 - k_0^2 \right] \tag{8}$$

$$p(r + \Delta r, t) = exp(ik_0 \Delta r) \prod_{j=1}^{n} \frac{1 + a_j \chi}{1 + b_j \chi} p(r, t) \tag{9}$$

In Eq. (13), Δz represents the thickness of the waveguide. Tu et al. (2022) provided the weak form of the differential equations involved in Eq. (9) and the process for minimizing the weighted residuals; thus, further elaboration is not provided herein. Based on the relationships in Eqs. (6) and (7), the discrete form χ can be obtained, allowing for the expression of Eq. (2) in Chebyshev spectral space.

$$\mathbf{X} = k_0^{-2} \left[\frac{4}{\Delta z^2} C_\rho D_N C_{1/\rho} D_N + C_{k^2} - k_0^2 I_N \right], \tag{10}$$

$$\widehat{\mathbf{p}}(r + \Delta r, t) = exp(ik_0 \Delta r) \prod_{j=1}^{n} \frac{1 + a_j \mathbf{X}}{1 + b_j \mathbf{X}} \widehat{\mathbf{p}}(r, t) \tag{11}$$

In Eq. (10), D_N is a matrix of order $N+1$, while C_ρ, $C_{1/\rho}$ and C_k^2 are the spectral coefficients for discretizing Chebyshev from physical space to spectral space. I_N is the unit matrix of order (N-1). Next, our primary focus is on solving the derived Eq. (11) using the solution process outlined as follows:

$$\prod_{j=1}^{n} (\mathbf{I}_N + b_j \mathbf{X}) \widehat{\mathbf{p}}(r + \Delta r, t) = exp(ik_0 \Delta r) \prod_{j=1}^{n} (\mathbf{I}_N + a_j \mathbf{X}) \widehat{\mathbf{p}}(r, t) \tag{12}$$

In each iteration step, it is necessary to solve a linear equation of the order $(N+1)$. The matrices were defined as $\mathbf{L}_\mathrm{j} = \mathbf{I}_\mathrm{N} + b_\mathrm{j}\mathrm{X}$, and $\mathbf{R}_\mathrm{j} = \mathbf{I}_\mathrm{N} + a_\mathrm{j}\mathbf{X}$. Let the propagation matrix T be defined as follows $\mathbf{T} = \prod_{j=1}^{n} \left(\mathbf{L}_j^{-1} \mathbf{R} \right)$; then, Eq. (12) can be expressed as:

$$\widehat{\mathbf{p}}(r + \Delta r, t) = exp(ik_0 \Delta r) \mathbf{T} \widehat{\mathbf{p}}(r, t) \tag{13}$$

Dur to the discontinuity in the vertical acoustic properties of seawater, and the requirement for smoothness in spectral methods, a single set of Chebyshev basis functions cannot accurately approximate the piecewise continuous sound speed, density, and attenuation. In this study, the domain decomposition method proposed by Min and Gottlieb (2005) was employed, which applies different numbers of Chebyshev basis functions for expansion and discretization across various layers. The depth operator and governing equations for the ℓ layer are given by:

$$\mathbf{X}_\ell = k_0^{-2} \left[\frac{4}{(h_\ell - h_{\ell-1})^2} C_{\rho_\ell} D_{N_\ell} C_{1/\rho_\ell} D_{N_\ell} + C_{k_\ell{}^2} - k_0^2 I_{N_\ell} \right], \tag{14}$$

$$\prod_{j=1}^{n} (\mathbf{I}_{N\ell} + b_j \mathbf{X}\ell) \widehat{\mathbf{p}}_\ell(r + \Delta r, t) = exp(ik_0 \Delta r) \prod_{j=1}^{n} (\mathbf{I}_{N\ell} + a_j \mathbf{X}_\ell) \widehat{\mathbf{p}}_\ell(r, t) \tag{15}$$

Because all layers must propagate forward, they should be assembled into a global matrix as follows:

$$\mathbf{X} = \begin{pmatrix} \mathbf{X}_1 & 0 & \dots & 0 \\ 0 & \mathbf{X}_2 \dots & 0 & \\ \vdots & \vdots & \vdots & \vdots \\ 0 & 0 & \dots & \mathbf{X}_\ell \end{pmatrix}, \widehat{\mathbf{p}} = \begin{pmatrix} \widehat{\mathbf{p}}_1 \\ \widehat{\mathbf{p}}_2 \\ \vdots \\ \widehat{\mathbf{p}}_\ell \end{pmatrix} \tag{16}$$

Global matrix $\mathbf{X}$ is an ordered diagonal matrix. By substituting the above equations, the initial sound pressure for the first segment was set as the sound pressure of the experimentally collected signal. After solving for the sound pressure at various depths in the first segment, the exit sound pressure at the flat seabed cutoff was used as the initial sound pressure for the next segment of the flat seabed, which was then iteratively solved.

4.2. Calculation results

The sound source was positioned as a far-field point source, with the sound pressure level at 50 m used as the source level. Receiver depths were set at 10 m and 20 m, with seawater and seabed treated as homogeneous media. The seawater density ρ is 1000 kg/m^3, and the sound speed, modeled using a shallow water negative gradient profile, ranges from approximately 1520 m/s to 1529 m/s, while the seabed is treated as a rigid interface. The total length of the seabed was 8 km, and the seabed attenuation coefficient was $0.311 \times (f/1000)^{1.75}$ dB/m. Fig. 6 shows the computed sound-field propagation characteristics of the wind farm. From the above signal analysis, we obtained the primary frequency-domain characteristics of the wind farm. The main frequency was 44 Hz, with discrete spectral peaks at 44, 88, 103, 176, and 206 Hz. In addition, a broadband sideband signal was observed at a peak frequency of 1050 Hz. Among them, 88 Hz and 176 Hz correspond to the 44 Hz fundamental frequency, 130 Hz corresponds to the 206 Hz fundamental frequency, and 1050 Hz corresponds to the peak frequency of the skirt-like spectrum. Fig. 7 presents the variation in noise with distance at four representative frequencies (44, 88, 130, and 1050 Hz). Fig. 6 illustrates the variation in noise with distance at the four frequencies.

At the low frequency of 44 Hz, owing to the longer wavelength, the sound waves propagate more smoothly. At receiver depths of 10 and 20 m, the sound field distribution exhibited a relatively uniform sound pressure level. As the frequency increased, more pronounced interference patterns appeared in the sound field, manifesting as fluctuations in the sound pressure levels. In addition, sound attenuation in seawater has become more significant. At a high frequency of 1050 Hz, the sound waves exhibited more intense interference effects. The sound field at receiver depths of 10 m and 20 m displayed highly complex fluctuation patterns, with the sound field rapidly attenuating at greater distances.

Through a comparative analysis of the developed model and experimental data, we thoroughly validated the sound propagation characteristics of the wind farm noise at different depths. However, in shallow-water environments, the distribution of sound propagation loss is significantly influenced by sea-surface conditions and seabed characteristics. An undulating seabed can concentrate and disperse sound-wave energy. These factors can affect the final computational results of numerical simulations. Although there were slight differences between the theoretical and experimental results due to approximation

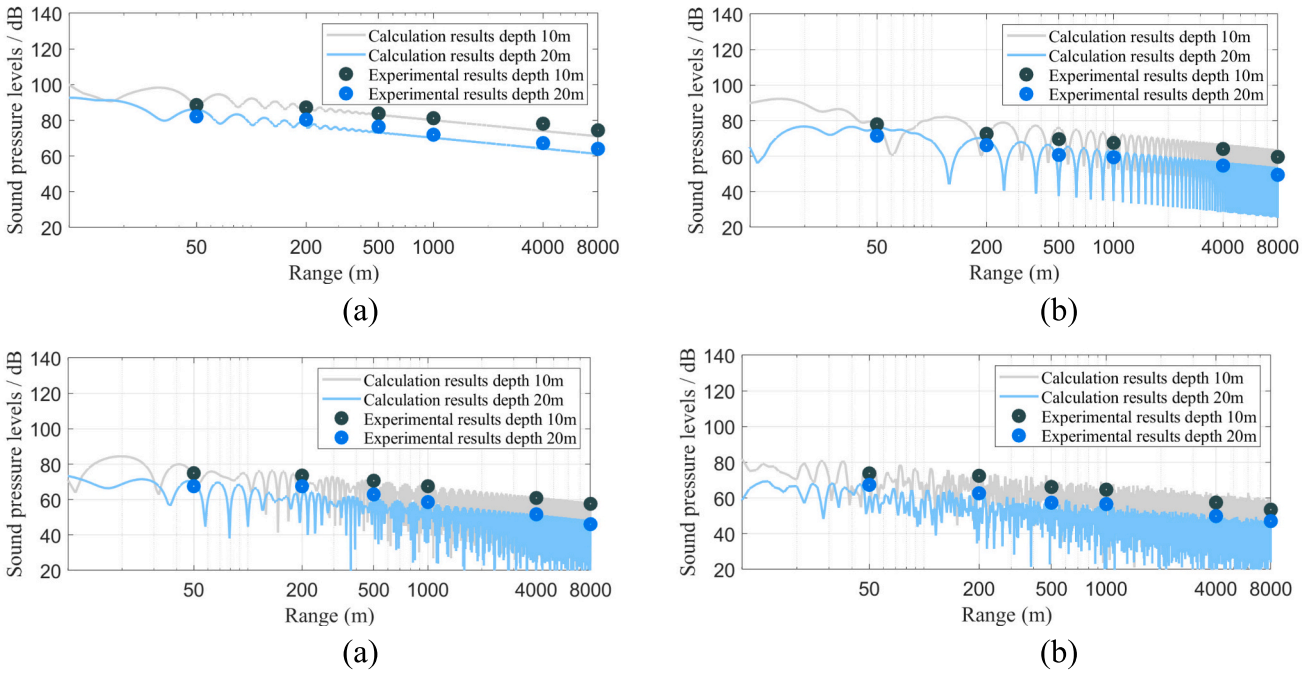

Fig. 6. Comparison of calculation results and experimental results: (a) 44 Hz; (b) 88 Hz; (a) 103 Hz; (a) 1050H.

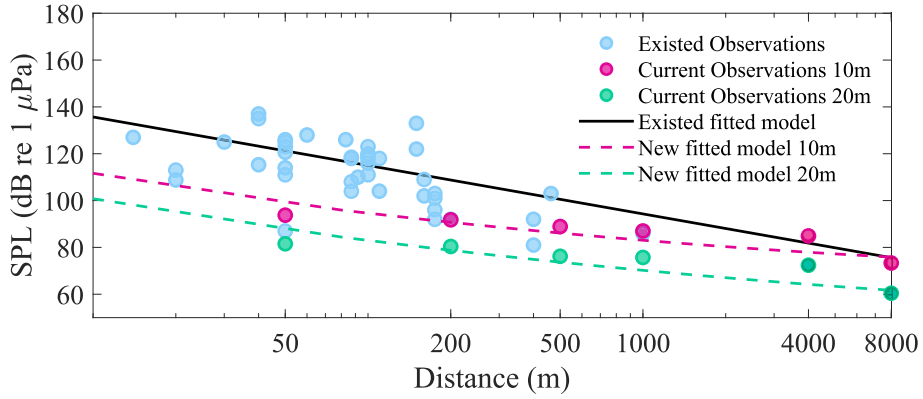

Fig. 7. Comparison of sound propagation models.

errors, both showed consistent peak positions and frequency trends. Overall, the experimental results are in good agreement with the theoretical calculations.

Fig. 6 clearly illustrates the complex characteristics of wind farm noise at the main frequency as it varies with distance and depth. Vertically, as the water depth increased from 10 m to 20 m, the attenuation characteristics of the wind farm noise showed significant differences. At the same distance, the noise pressure levels were generally lower in deeper water than in shallower water. This reflects additional attenuation due to factors such as medium absorption, scattering, and boundary effects in deeper waters. Horizontally, for all tested depths, the main frequency sound pressure level of the windfarm noise decreased significantly with increasing distance. When the distance exceeded 4 km, the noise level gradually approached background ocean noise. This indicates that beyond this distance, the impact of the wind farm noise on the marine environment is minimal.

5. Discussion

This study aimed to explore the characteristics of underwater operational noise from offshore wind turbines as a function of wind speed, as well as to conduct a preliminary survey to assess the impact of underwater noise from offshore wind farms on marine ecosystems. All measurements were taken at a 5.5 MW wind turbine located on Nanpeng Island in Yangjiang, Guangdong Province, China. The preliminary data analysis indicated that the underwater noise intensity generated by the wind farm was primarily concentrated in the frequency range below 1500 Hz.

For further analysis, the observed noise was divided into two main frequency bands. Field measurements have shown that the operational noise from a wind farm is predominantly generated by mechanical vibrations (Yang et al., 2018; Yoon et al., 2023). Marmo et al. (2013) found through simulations and experimental analysis that mechanical vibrations typically exhibit tonal rather than broadband characteristics. Low-frequency signals from gear meshing typically occur below 50 Hz, while noise from electromagnetic ranges from 50 Hz to 2 kHz. The resonance modes on the turbine surface are generally related to multiple gear meshing frequencies. Therefore, some of the noise in this experiment included fundamental frequency pulses and modulated spectra with discrete line spectrum characteristics, showing peak frequencies at

44, 88, 103, 176, and 206 Hz (where 88 Hz and 176 Hz are multiples of 44 Hz, and 206 Hz is a multiple of 103 Hz). Another component of the noise included a continuous band spectrum with sound pressure levels significantly higher than the ambient marine background noise, occurring in the frequency range of 500–1500 Hz.

Near the turbine, within 50 m, the frequency spectrum drops suddenly around 1500 Hz. This phenomenon can be attributed to the differences in the turbine models and capacities; the noise bandwidth observed in this study is broader than that of the 3.0 MW and 3.6 MW turbines. This contrasts with Yoon et al. (2023) and Pangerc et al. (2016), who noted wind farm noise frequencies below 1 kHz. According to Wenz (1936), the spectral distribution of ocean ambient noise is primarily derived from wind-driven sea-surface noise and vessel noise. The energy distribution of wind-driven sea-surface noise spans the frequency range of 10–20 kHz, whereas the major contributions of vessel noise are concentrated below 1 kHz. The background noise above 1 kHz is mainly caused by hydrodynamic exchanges due to wind. However, this is not absolute because the turbine capacity and dimensions in the experimental area are significantly greater than those of previous turbines, potentially generating noise frequencies that reach up to 1500 Hz, thereby masking wind-induced noise within this frequency band. This also explains the significant decrease in the sound intensity at frequencies above 1500 Hz.

5.1. Acoustic propagation characteristics

Noise levels measured from existing data (Betke et al., 2004; Elmer et al., 2007; Nedwell et al., 2024; Thomsen et al., 2015) show that offshore wind turbine noise is low in both absolute and relative terms. The measurements show that the noise levels were comparable to or less than 1 km. Tougaard's extensive experiments and observations have provided a linear model for estimating the total sound pressure level. This model plots sound pressure against distance, wind speed, and turbine size (measured in megawatts). The model equation is: $L_{eq} = C + \alpha \log_{10}(\text{Range}/100\ \text{m}) + \beta \log_{10}(\text{Wind Speed}/10\ \text{m/s}) + \gamma \log_{10}(\text{TurbineSize}/1\ \text{M/W})$. where wind speed and turbine size are identified as two additional significant factors affecting noise levels. The constants are obtained from extensive observations with $C = 115$, $\alpha = -20.7$, $\beta = 1$, $\gamma = 1$. Fig. 7 shows a simplified model of sound propagation in wind farms. The black curve represents the theoretical formula, whereas the blue dots represent observational data from previous studies.

However, most modern turbines are designed for greater capacity and are significantly optimized. Therefore, the fitting formulae presented in previous studies are no longer applicable. The noise level estimation model provided in this study, which describes the variation in underwater noise with distance, is given by Eq. (17).

$$SPL = a(log_{10}(Range))^2 + b(log_{10}(Range))^2 + c(TurbineSize/1M/W) + (Depth/10)log_{10}(WindSpeed) \quad (17)$$

In Eq. (9), $a = 1.8149$, $b = -21.2215$, $c = 22.9933$, where Range represents the distance, *TurbineSize* denotes the turbine capacity, *Depth* indicates the depth, and *WindSpeed* is the wind speed. Fig. 7 shows the blue dots for wind farm noise levels obtained from previous studies. The black line represents the fitting formula obtained from previous studies. The pink and green dots represent the sound pressure levels of the windfarm noise measured at different water depths in the current experiment. Although these data showed a consistent trend in noise variation with distance, there were significant differences in the sound pressure levels. The pink and green curves obtained by fitting the new experimental data better match the actual observations. In contrast, the newly fitted model provided significantly improved prediction performance at different water depths.

It is important to clarify that the fitted model incorporates factors such as seabed topography and weather conditions, as previously described. When applying this model, the following assumptions are made: the seabed density and sound speed are considered uniform, with seabed elasticity neglected; and the sound speed and density of seawater are assumed to be laterally uniform. When these parameters vary, the model's applicability and prediction accuracy cannot be reliably ensured. This limitation is inherent to empirical model fitting, particularly under complex environmental conditions, where simple empirical models often fall short in capturing the multiple factors influencing underwater acoustic characteristics.

5.2. The impact of wind farm noise on marine life

The communication frequency range of marine mammals and fish often overlap with the low-frequency noise produced by wind farms. This can make their habitats less suitable, limit communication ranges between individuals, and potentially affect their natural behavior in the long term (Mooney et al., 2020). Furthermore, a quiet acoustic environment is essential for monitoring marine life using passive acoustic methods (Dario et al., 2024).

However, studies in the Netherlands suggest that with proper wind farm siting, negative impacts on marine life can be minimized and may even promote biodiversity (Bennun et al., 2021). Wilhelmsson et al. (2006) found that blue mussel growth on wind turbines increased the abundance of fish and benthic animals around wind farms. According to Maar et al. (2009), wind turbines provide ample habitat for mussels, effectively doubling the filter-feeding biomass within a wind farm. Köller et al. (2006) suggested that an increase in mussel biomass can accelerate the food chain, potentially reducing water turbidity and promoting the growth of phytoplankton and filamentous algae. Lindeboom et al. (2011) found that wind farms provide essential rest and shelter areas for fish and marine mammals, increasing species richness by 37 species in the vicinity. The biomass of species such as pollock, cod, and bream increases significantly near wind farms, providing ample food sources for marine mammals. Overall, the diversity, abundance, and biomass of the benthic communities around offshore wind farms may gradually increase over time.

Repeated, long-term noise exposure poses a cumulative risk to marine mammals. Auditory perception is vital for animals, including mammals and fish, as sound can travel great distances underwater. Marine animals, which have a hearing range and sound production capacity far surpassing those of humans, can detect these sounds. Research by Stafford (2013) and Mellinger et al. (2007) suggested that human-generated sound frequencies overlap with the frequency ranges used by marine animals (Fig. 8). Consequently, the production and reception of sound are crucial for the survival of marine species.

Combining experimental data with the communication and behavioral frequency ranges of marine animals, Fig. 8 illustrates that most marine mammals are more sensitive to medium and high-frequency noise. However, wind turbine noise is predominantly low frequency, which lessens its direct impact on these animals. In contrast, low-frequency noise could considerably affect sensitive species like fish. Particularly near wind turbines, low-frequency noise may disrupt essential behaviors such as reproduction, foraging, and predator avoidance. Sea turtles, whose communication and auditory frequency ranges are narrowly focused in the low-frequency range, experience substantial overlap with wind farm noise, potentially impacting their auditory perception and behavior. For fish, whose communication frequencies also fall mainly within the low-frequency range, wind turbine noise overlaps significantly. This overlap suggests that wind farm noise may mask essential physiological activities for fish, such as breeding and feeding. Therefore, when assessing the impact of wind farms on marine life, the focus should be on species sensitive to low-frequency noise, particularly fish and sea turtles, whose behaviors are more susceptible to disruption from low-frequency noise.

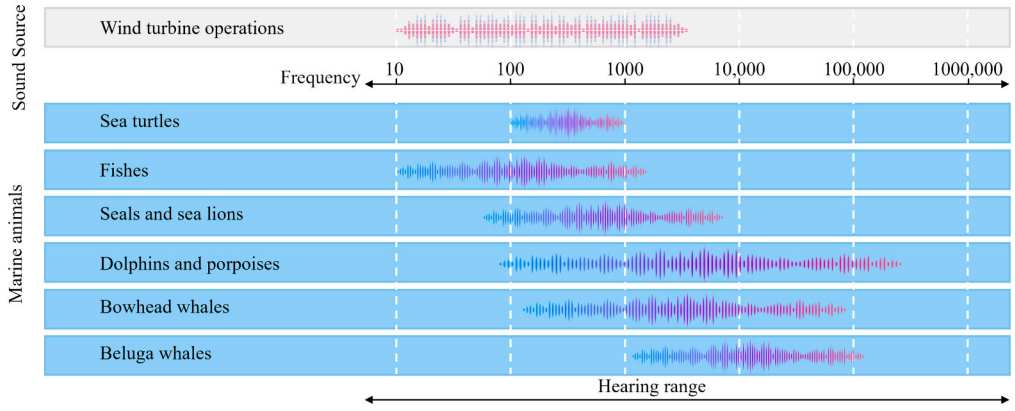

Fig. 8. Frequency ranges of marine animals and noise.

6. Conclusions

An experimental study of underwater noise characteristics was conducted at the Yangjiang offshore wind farm during its operational phase. The goal of this study was to gain a better understanding of how underwater noise propagates in the presence of wind farms. This study aims to provide a reference for the safety and demarcation of warning lines in fishing areas. This study yielded the following conclusions:

(1) Attenuation characteristics: In the study area, fixed-base wind turbines produce primarily low-frequency noise. Gearboxes and bearings, as well as the resonance of underwater structures, are the primary sources of this noise. This low-frequency noise causes slower attenuation in water, resulting in greater energy decay distance. Experimental data show that, when compared to the noise levels within 50 m of the wind turbine, the sound propagation loss within 1 km is approximately 10 dB. However, beyond 1 km, the sound pressure level of the noise signal dropped significantly, with the sound propagation loss reaching 10–20 dB.
(2) Spectral characteristics: The wind farm operation generated relatively low underwater noise. The acoustic energy was primarily concentrated below 1500 Hz with both discrete and sideband spectra. The primary frequency of the discrete spectrum was 44 Hz with harmonics at 88 and 176 Hz. The sideband spectrum peaks at approximately 1050 Hz, forming a skirt-shaped pattern. Beyond 4 km, the impact of the wind noise becomes negligible.
(3) Validation of sound propagation properties using the spectral parabolic equation and experimental Data: The comparison of calculated distance intensity and measured data confirmed that the sound propagation model is consistent with the experimental results. This resulted in a refinement of the attenuation formula for turbine noise based on distance.

In summary, this study comprehensively elucidated the underwater noise characteristics of the Yangjiang offshore wind farm by analyzing the noise characteristics at multiple sites. The results provide crucial empirical and theoretical foundations for understanding underwater noise generation. Their spatiotemporal distribution patterns and relationships with external factors were revealed. This study also serves as a reference for determining the safe distances between fishing areas and offshore wind farms.

Funding

This work was supported by the GuangDong Basic and Applied Basic Research Foundation - Offshore Wind Power Joint Foundation [project number 2023A1515240013]; and GuangDong Basic and Applied Basic Research Foundation [project number 2022A1515011067]; and National Natural Science Foundation of China [grant number 11974084].

Credit authorship contribution statement

Xinze Huo: Specifically performing the experiments and data collection, analysis results, and preparation of the manuscript. Conceptualization, Formal analysis, Investigation, Writing - original draft, *V*isualization. **Peizhen Zhang:** corresponding author, experiment - detailed description, conceptual design, and ideas. Specifically performing the experiments, and data collection, analysis of results, preparation of manuscript. Conceptualization, Formal analysis, Investigation, Methodology, Project administration, Writing - review & editing. **ZiYi Feng:** Data collection, and Investigation.

Declaration of competing interest

There are no conflicts to declare.

Data availability

We have uploaded the dataset and code for this study to GitHub and Google Drive.

The dataset can be downloaded from the following link: https://drive.google.com/drive/folders/1l9huwn1pwwQua61sqzLgUJOYOh9DG7Xr?usp=sharing.

The code can be downloaded from the following link: https://github.com/1ecin1/Sound_Propagation.

References

Andersson, M.H., 2011. Offshore Wind Farms-Ecological Effects of Noise and Habitat Alteration on Fish. Department of Zoology: Stockholm University.
Andrea, C., Fabio, M.Z., Alessandro, D.P., Andrea, L., 2021. Effect of the uneven blade spacing on the noise annoyance of axial-flow fans and side channel blowers. Appl. Acoust. 177, 107924. https://doi.org/10.1016/j.apacoust.2021.107924.
Bartłomiej, S., Tadeusz, Dominik M., Paweł, M., Paweł, P., Maciej, K., Marcjanna, C., 2024. Suitability analysis of selected methods for modelling infrasound and low-frequency noise from wind turbines. Energies 17 (12), 2832. https://doi.org/10.3390/en17122832.
Bennun, L., van Bochove, J., Ng, C., Fletcher, C., Wilson, D., Phair, N., Carbone, G., 2021. Mitigating Biodiversity Impacts Associated with Solar and Wind Energy Development. Guidelines for Project Developers. Gland, Switzerland: IUCN and Cambridge, UK. TheBiodiversity Consultancy.
Betke, K., Glahn, M.S., Matuschek, R., 2004. Underwater noise emissions from offshore wind turbines. In: CFA/DAGA'04 Conference, Strasbourg, 22–25, pp. 591–592.
Betke, K., Glahn, S.V., Matuschek, R., 2005. Underwater noise emissions from offshore wind turbines. Int. Meet. Wind Turb. Noise 18 (2), 25–30.
Boško, J., Ljubiša, B., Božidar, M., Danijela, S., Nikola, S., 2023. Cumulative impact of wind farm noise. Appl. Sci. 13 (15), 8792. https://doi.org/10.3390/app13158792.
Buckingham, M.J., 1992. Ocean-Acoustic Propagation Models. Physics Editions, Les Ulis, France.

Colas, J., Emmanuelli, A., Dragna, D., Blanc-Benon, P., Cotté, B., JAM S R., 2023. Wind turbine sound propagation: comparison of a linearized Euler equations model with parabolic equation methods. J. Acoust. Soc. Am. 154 (3), 1413–1426.
Collins, M.D., 1993. A split-step padé solution for the parabolic equation method. J. Acoust. Soc. Am. 93 (4), 1736–1742. https://doi.org/10.1121/1.406739.
Collins, M.D., 1994. Generalization of the split-step Padé solution. J. Acoust. Soc. Am. 96 (1), 382–385. https://doi.org/10.1121/1.410488.
Dario, D., Samir, R., Rajesh, S., Sean, S., Bhupendra, R., Scott, C., Pete, B., Nicola, F., 2024. Acoustic fingerprints in nature: a self-supervised learning approach for ecosystem activity monitoring. Eco. Inform. 83 (102823), 1574–9541.
De Oliveira, R.F., de Araujo, L.A.F., Zaffaroni, C.V., de Moura, G.B., 2023. Wind farm noise and anuran diversity patterns: a case study in Brazilian seasonal dry tropical forest. Bioacoustics 32 (5), 544–555. https://doi.org/10.1080/09524622.2023.2204325.
Elmer, K.H., Betke, K., Neumann, T., 2007. End Report of the BMU Research Project 0329947. Standard Procedure for Determining and Evaluating the Pollution of the Marine Environment Due to the Noise Emissions of Offshore Wind Energy Plants. Hannover, Germany.
Etter, P.C., 2018. Underwater Acoustic Modeling and Simulation. CRC Press, Boca Raton, FL.
Feng, X., Chen, C., Yang, K., 2024. Fast estimation algorithm of sound field characteristics under the disturbance of sound speed profile in the marine environment. Ocean Eng. 2024 (297), 117197. https://doi.org/10.1016/j.oceaneng.2024.117197.
Fricke, M.B., Rolfes, R., 2015. Towards a complete physically based forecast model for underwater noise related to impact pile driving. J. Sound Vib. 137 (3), 1564–1575.
General Administration of Quality Supervision, 2009. Inspection and Quarantine of the People's Republic of China.
Gilbert, K.E., White, M.J., 1989. Application of the parabolic equation to sound propagation in a refracting atmosphere. J. Acoust. Soc. Am. 85 (2), 630–637.
He, R., Tsouvalas, A., Xu, X.M., Dong, L.J., 2023. Editorial: noise and vibrations in offshore wind farms and their impact on aquatic species. Front. Mar. Sci. 2023 (10), 1293733. https://doi.org/10.3389/fmars.2023.1293733.
He, T.J., Liu, J., Ye, S.J., Qing, X., Mo, S.Q., 2024. A novel model order reduction technique for solving horizontal refraction equations in the modeling of three-dimensional underwater acoustic propagation. J. Sound Vib. 2024 (591), 118617. https://doi.org/10.1016/j.jsv.2024.118617.
Jensen, F.B., Kuperman, W.A., Porter, M.B., Schmidt, H., 2011. Computational Ocean Acoustics. Springer-Verlag, New York.
Köller, J., Köppel, J., Peters, W., 2006. Offshore Wind Energy Research on Environmental Impacts. Springer-Verlag, Berlin Heidelberg, p. 371.
Lindeboom, H.J., Kouwenhoven, H.J., Bergman, M.J.N., Bouma, S., Brasseur, S., Daan, R., Fijn, R.C., de Haan, D., Dirksen, S., van Hal, R., Hille Ris Lambers, R., ter Hofstede, R., Krijgsveld, K.L., Leopold, M., Scheidat, M., 2011. Short-term ecological effects of an offshore wind farm in the Dutch coastal zone; a compilation. Environ. Res. Lett. 6, 035101.
Lippert, T., Lippert, S., 2012. Modelling of pile driving noise by means of wavenumber integration. Acoustics Australia 3, 178–182.
Liu, D., Li, Z.L., Liu, R.Y., 2021. Sound propagation in shallow water with periodic rough bottom. Acta Phys. Sin. 70 (3), 034302.
Lou, Y.J., Ma, J., 2024. Numerical simulation of underwater noise of offshore wind turbine. J. Dalian Univ. Technol. 64 (03), 292–300.
Maar, M., Bolding, K., Petersen, J.K., Hansen, J.L.S., Timmermann, K., 2009. Local effects of blue mussels around turbine foundations in an ecosystem model of Nysted offshore wind farm, Denmark. J. Sea Res. 62, 159–174.
Madsen, P.T., Wahlberg, M., Tougaard, J., 2006. Wind turbine underwater noise and marine mammals: implications of current knowledge and data needs. Mar. Ecol. Progress 309 (8), 279–295. https://doi.org/10.3354/meps309279.
Marmo, B., Roberts, I., Buckingham, M.P., King, S., Booth, C., 2013. Modelling of noise effects of operational offshore wind turbines including noise transmission through various foundation types. Edinburgh Scott. Govern. 4 (5), 100.
Mellinger, D.K., Kathleen, S., Sue, M., Robert, D., Haru, M., 2007. An overview of fixed passive acoustic observation methods for Cetaceans. Oceanography 20 (4), 37–45.
Min, M.S., Gottlieb, D., 2005. Domain decomposition spectral approximations for an eigenvalue problem with a piecewise constant coefficient. SIAM J. Numer. Anal. 43, 502–520.
Mooney, T.A., Andersson, M.H., Stanley, J., 2020. Acoustic impacts of offshore wind energy on fishery resources: an evolving source and varied effects across a wind farm's lifetime. Oceanography 33 (4), 82–95.
Nedwell, J.R., Brooker, A.G., Edwards, B., Bird, H., 2024. Subsea operational noise assessment of the Lynn and Inner Dowsing Offshore Wind Farm Sites, Report No. E273R0118 to COWRIE Ltd., Subacoustech Ltd., Southampton, UK.
Pangerc, T., Theobald, P.D., Wang, L.S., Robinson, S.P., Lepper, P.A., 2016. Measurement and characterisation of radiated underwater sound from a 3.6 MW monopile wind turbine. J. Acoust. Soc. Am. 140, 2913–2922.
Peng, Y.X., Jarquin, L.A., Tsouvalas, A., 2023. A multi-physics approach for modeling noise mitigation using an air-bubble curtain in impact pile driving. Front. Mar. Sci. 10, 1134776.
Qian, J.Y., Lin, D.Q., Xing, B.B., Gong, D.H., Guo, J.L., Liu, Y.T., Li, Z.M., Yin, L.M., 2022. Potential impact of noise from underwater tunnel during metros operation on aquatic organisms. J. Dalian Ocean Univ. 37 (02), 329–337.
Rami, E.D., Okko, O., Harri, K., 2024. Anthropogenic underwater noise: A review on physiological and molecular responses of marine biota. Mar. Pollut. Bull. 199, 0025-326x.
Reinhall, P.G., Dahl, P.H., 2011. Underwater Mach wave radiation from impact pile driving: theory and observation. J. Acoust. Soc. Am. 130 (3), 1209–1216.
Sergeev, V.A., 2024. On the upslope propagation of an Adiabatic normal mode in a Wedge-Shaped Sea. Russ. J. Math. Phys. 31 (2), 308–314.
Southall, B.L., Tollit, D., Amaral, J., Clark, C.W., Ellison, W.T., 2023. Managing human activity and marine mammals: a biologically based, relativistic risk assessment framework. Front. Mar. Sci. 10, 1090132.
Stafford, K., 2013. Anthropogenic Sound and Marine Mammals in the Arctic.
Su, Y.Y., 2023. Research on Vibration Transmission Characteristics of Offshore Wind Turbine Supporting Structure. Tianjin University.
Sun, P.L., Li, X.P., Zhao, H.Y., Ma, S.Q., Liu, W.J., Zhou, M.Q., 2022. Research on the noise characteristics of Wind Turbine. Environ. Monitor. China 38 (02), 129–135.
Thomsen, F., Gill, A., Kosecka, M., Andersson, M., Andre, M., Degraer, S., Folegot, T., Gabriel, J., Judd, A., Neumann, T., Norro, A., Risch, D., Sigray, P., Wood, D., Wilson, B., 2015. MaRVEN-Environmental impacts of noise, vibrations and electromagnetic emissions from marine renewable. In: Final Project Report to the European Commission, Directorate-General for Research and Innovation.
Tougaard, J., Hermannsen, L., Madsen, P.T., 2020. How loud is the underwater noise from operating offshore wind turbines? J. Acoust. Soc. Am. 148 (5), 2885–2893. https://doi.org/10.1121/10.0002453.
Tsouvalas, A., 2020. Underwater noise emission due to offshore pile installation: a review. Energies 13, 3037. https://doi.org/10.3390/en13123037.
Tu, H., Wang, Y., Ma, X., Zhu, X., 2022. Applying the Chebyshev–Tau spectral method to solve the parabolic equation model of wide-angle rational approximation in ocean acoustics. J. Theoretic. Comp. Acoust. 30 (2), 2150013. https://doi.org/10.1142/S2591728521500134.
Tu, H.W., Wang, Y.X., Zhang, Y.U., Wang, X.D., Liu, W., 2023. A spectrally discretized wide-angle parabolic equation model for simulating acoustic propagation in laterally inhomogeneous oceans. J. Acoust. Soc. Am. 153 (6), 3334. https://doi.org/10.1121/10.0019748.
Vegu, S.R.K.K., Stephen, B., 2024. Visual analysis of oceanic data for marine ecosystems. Ecol. Inform. 82 (102), 762, 1574–9541.
Wahlberg, M., Westerberg, H., 2005. Hearing in fish and their reactions to sound from offshore wind farms. Mar. Ecol. Progress 288 (1), 295–309. http://www.jstor.org/stable/24867983.
Wang, W.J., Liu, Y.D., Qi, C., Zhang, B., 2014. Classification and seasonal variability of the sound velocity spring layer in the South China Sea. Mar. Sci. 38 (08), 82–93.
Wang, C.H., Tao, Y., Xu, X.M., 2022. Simulation research on underwater noise of offshore wind farm during operation period. Conf. Pap. 429–431.
Wang, C.J., Pan, H.D., Wang, G.L., Wang, Y.F., 2024. Wind-generated characteristics of ambient noise in Southeastern Indian Ocean Based on Underwater Glider Observation. Adv. Mar. Sci. 42 (01), 160–169.
Wenz, G.M., 1936. Acousticambient noise in the ocean: spectra and sources. J. Acoust. Am. 34, 1936–1956.
Wilhelmsson, D., Malm, T., Öhman, M.C., 2006. The influence of offshore windpower on demersal fish. ICES J. Mar. Sci. 63, 775–784.
Yang, C.M., Liu, Z.W., Lü, L.G., Yang, G.B., Huang, L.F., Jiang, Y., 2018. Observation and comparison of tower vibration and underwater noise from offshore operational wind turbines in the East China Sea Bridge of Shanghai. J. Acoust. Soc. Am. 144 (6), EL522–EL527.
Yoon, Y.G., Han, D.-G., Choi, J.W., 2023. Measurements of underwater operational noise caused by offshore wind turbine off the southwest coast of Korea. Front. Mar. Sci. 10, 1153843.
Zhu, H.H., Zhu, J., Tang, J., Zhang, H.G., Zheng, G.X., 2020. Effects of sediment acoustic characteristics on low- frequency acoustic field distribution in shallow water. Acta Acustica 45 (5), 664–674.